

1 Reliability of chemical microanalyses for solid waste materials

2
3 Vojtěch Ettler^{1*}, Zdenek Johan², Martina Vítková¹, Roman Skála^{1,3},
4 Marek Kotrly⁴, Gerlinde Habler⁵, Mariana Klementová⁶

- 5
6
7 1. Institute of Geochemistry, Mineralogy and Mineral Resources, Charles University in
8 Prague, Faculty of Science, Albertov 6, 128 43 Prague 2, Czech Republic (e-mail:
9 ettler@natur.cuni.cz, fax. +420 221951496, telephone +420 221951493)
10 2. Bureau des Recherches Géologiques et Minières (BRGM), av. Claude Guillemin, 45060
11 Orléans, cedex 2, France
12 3. Institute of Geology of the Academy of Sciences of the Czech Republic, v.v.i., Rozvojová
13 269, 165 00 Prague 6, Czech Republic
14 4. Institute of Criminalistics Prague, P.O. box 62/KUP, Strojnická 27, 170 89 Prague 7,
15 Czech Republic
16 5. Department of Lithospheric Research, University of Vienna, Althanstrasse 14, A-1090
17 Vienna, Austria
18 6. Institute of Inorganic Chemistry of the AS CR, v.v.i., 250 68 Husinec-Řež, Czech
19 Republic

20
21 * corresponding author
22
23
24

25 Abstract

26 The investigation of solid speciation of metals and metalloids is required for accurate
27 assessment of the hazardous properties of solid waste materials from high-temperature
28 technologies (slag, bottom ash, fly ash, air-pollution-control residues). This paper deals with
29 the problem of reliability of microanalyses using a combination of electron microprobe
30 analysis (EPMA) and scanning electron microscopy (SEM) only. These methods do not
31 permit to detect nanophases in host-crystals and lead to erroneous interpretation of analytical
32 results, considering the elements of nanophases as belonging to the crystal structure of the
33 main phase. More detailed analysis using transmission electron microscopy (TEM) on foils
34 prepared by focused ion beam (FIB) can be used to solve this analytical problem. In this

1 study, lamellar aggregates of potassium-rich clinopyroxenes were detected in copper smelting
2 slags by a combination of SEM and EPMA. However, FIB-TEM indicated the presence of
3 leucite inclusions (tens to hundreds nm in size) within the clinopyroxene lamellae. Based on
4 examples from smelting slags and other solid waste materials, recommendations for standard
5 SEM and EPMA applications and the need for methods with higher resolution for
6 mineralogical investigation of waste materials are discussed.

7

8 **Keywords:** solid speciation, contaminants, electron probe microanalysis, FIB-TEM, slag

9

10 **1. Introduction**

11 The knowledge of detailed mineralogical and chemical compositions of solid phases is
12 crucial for the assessment of hazardous properties in solid waste materials [1]. During the
13 past decade, an increasing number of papers has been devoted to mineralogical investigations
14 of waste materials from numerous high-temperature technologies, including metallurgical
15 slags and mattes [2–13], bottom and fly ashes from municipal solid waste incinerators
16 (MSWI) [14,15] or solid residues from sewage sludge gasification [16]. Scanning electron
17 microscopy (SEM) coupled to energy dispersion spectrometry (EDS) and electron probe
18 microanalysis (EPMA) are often used to determine the chemical compositions of various
19 phases. The beam size of these techniques is generally close to 1 μm ; however the volume of
20 the analyzed material is generally in the range of several μm^3 according to the analytical
21 conditions (beam current and beam accelerating voltage) and the nature of the specimen [17].
22 The general formula of the clinopyroxene (Cpx) is $\text{M}_2\text{M}_1\text{T}_2\text{O}_6$, where T is a tetrahedral site
23 occupied mostly by Si and Al, whereas other cations enter the M2 and M1 sites [18 and
24 references therein]. During our recent investigation of copper slags from the Zambian

1 Copperbelt [12], we noticed the presence of potassium-rich Cpx. Potassium with ionic radius
2 of 1.51 Å [19] was thought to be too large to enter the Cpx structure at ambient pressures. At
3 higher pressures (>5 GPa), it was observed that potassium can substitute for Ca²⁺ or Mg²⁺ in
4 the M2 site [18], which is, however, not possible for slags produced at ambient pressures. In
5 this context, we carried out a more detailed study using a combination of other methods with
6 significantly higher spatial resolution (focused ion beam technique coupled to transmission
7 electron microscopy, FIB-TEM). Our data presented in this paper show how tricky the
8 chemical determinations of phases in solid wastes can be, with particular implications and
9 recommendations for the solid speciation of hazardous elements, such as metals and
10 metalloids.

11

12 **2. Experimental methods**

13 The slag samples came from the Nkana slag dumps in the Zambian Copperbelt (S12°50'20'',
14 E 28°12'40'') and occurred as heavy and dense fragments up to 7 cm in size of black to gray
15 color. The samples were prepared as polished thin sections for microscopic observation and
16 electron probe microanalysis. A TESCAN VEGA scanning electron microscope equipped
17 with an Oxford Link X-Max 50 energy dispersion spectrometer at Charles University in
18 Prague (Czech Republic) was used for imaging and semi-quantitative chemical analyses.
19 Quantitative microanalyses were performed using a Cameca SX-100 electron microprobe
20 (EPMA) at the Institute of Geology, Academy of Sciences of the Czech Republic, Prague.
21 The following measurement conditions were used for the EPMA of silicate phases:
22 accelerating voltage 15 kV, beam current 4 nA (low current used to avoid volatilization of
23 alkalis), counting time 10 s and spot size 1 µm; standards used: jadeite, NaAlSi₂O₆ (Na,
24 Kα), quartz, SiO₂ (Si, Kα), synthetic Al₂O₃ (Al, Kα), sanidine, (K,Na) AlSi₃O₈ (K, Kα),

1 diopside, $\text{CaMgSi}_2\text{O}_6$ (Ca, $K\alpha$), rutile, TiO_2 (Ti, $K\alpha$), hematite, Fe_2O_3 (Fe, $K\alpha$), Mn Cr
2 spinel, MnCr_2O_4 (Cr, $K\alpha$), periclase, MgO (Mg, $K\alpha$), cobalt metal (Co, $K\alpha$). Empirical
3 formulae of Cpx were calculated on 4 cations per formula unit and the ferric and ferrous iron
4 contents were estimated assuming charge balance with 6 oxygens per formula unit. To verify
5 the presence of potassium in the Cpx at higher spatial resolution, three foils for transmission
6 electron microscopy (TEM) have been prepared using a FEI Quanta 3D FEG Dual Beam
7 focused ion beam (FIB) instrument at the Department of Lithospheric Sciences at the
8 University of Vienna (Austria). The instrument is equipped with a Field Emission Gallium
9 source. Platinum was used as deposition material for surface grounding and mounting the foil
10 onto a Cu-grid. Throughout the sputtering and deposition processes, the ion-beam
11 accelerating voltage was 30 kV, whereas successively lower beam currents (ranging from 50
12 nA to 30 pA) were used for progressive milling steps. Foils with dimensions of $17\ \mu\text{m} \times 10$
13 $\mu\text{m} \times 2\ \mu\text{m}$ were cut with a well-defined orientation perpendicular to the Cpx-lamellae. The
14 foils were transferred to a Cu-grid by in-situ lift-out using an Omniprobe 100.7
15 micromanipulator. Then, the final thinning was performed stepwise using beam currents of
16 500 pA, 300 pA, 100 pA and finally 30 pA. The final thinned foil area was $13\ \mu\text{m} \times 9\ \mu\text{m}$ in
17 size and 90–160 nm thick. For subsequent TEM investigations presented in this paper, we
18 used the thinnest area located close to the center of foil #2 with thickness close to 90 nm. The
19 TEM investigations on FIB-prepared foils were carried out on a JEOL JEM 3010 microscope
20 operated at 300 kV (LaB₆ cathode, point resolution 1.7° A) with an attached Oxford
21 Instruments energy dispersive X-ray spectrometer (EDS) at the Institute of Inorganic
22 Chemistry, Academy of Sciences of the Czech Republic. The images were recorded on a
23 CCD camera with resolution of 1024×1024 pixels using the Digital Micrograph software
24 package. The EDS analyses were acquired and treated in the INCA software package.

1 Selected area electron diffraction (SAED) patterns were evaluated using the Process
2 Diffraction software package [20].

3

4 **3. Results and discussion**

5 Previous studies using powder X-ray diffraction analysis (XRD), EPMA and SEM
6 investigations indicated that Cpx and spinels were the predominant phases in the studied
7 slags, often associated with minor olivine-type phases and leucite [12]. Whereas Cpx and
8 olivines often formed large skeletal or harissitic crystals (up to several hundred μm in size),
9 leucite and spinels formed globular and well-delimited crystals, generally up to 100 μm in
10 size [12]. In the slag sample, where K-Cpx was detected, Cpx forms approximately 1 mm
11 wide, plume-shaped lamellar aggregates stacked in zones (Fig. 1a). Such spinifex textures
12 indicate the quenching of the slag melt and rapid crystallization of Cpx. Individual Cpx
13 crystallites were approximately 1–2 μm wide (Fig. 1b) and only larger lamellae were
14 selected for the EPMA analyses. The EPMA indicate that the Cpx crystallites are enriched in
15 K (Table 1). The maximum K concentration in Cpx was 2.88 wt% K₂O (corresponding to
16 0.146 atoms per formula units, apfu) in the core of lamellae of the plume-like crystals (spot 2,
17 Fig. 1b). The EPMA of this KCpx yielded the formula
18 $(\text{Ca}_{0.802}\text{K}_{0.146}\text{Fe}^{2+}_{0.030}\text{Na}_{0.020})_{\Sigma 1.000}(\text{Fe}^{2+}_{0.661}\text{Fe}^{3+}_{0.290}\text{Mg}_{0.226}\text{Al}_{0.100}\text{Co}_{0.042}\text{Ti}_{0.018})_{\Sigma 1.000}(\text{Si}_{1.742}$
19 $\text{Al}_{0.258})_{\Sigma 2.000}\text{O}_{6.000}$.

20 However, the FIB-TEM investigation showed that Cpx lamellae are intimately associated
21 with leucite (KAlSi₂O₆). Leucite inclusions of variable size (tens to hundreds of nm) and
22 Cpx–leucite inter-growths were not visible on the SEM images, but were detected by TEM
23 coupled to EDS and SAED (Fig. 2). EDS spot analyses as well as X-ray elemental mapping
24 performed on the thinned foils indicate that K is not present in the clinopyroxene crystal

1 structure but is exclusively related to the associated leucite (Fig. 2). This study indicates that
2 EPMA analyses provided the chemical compositions of Cpx, which are flawed due to the
3 presence of nanometer-size solid inclusions and intergrowths with a K-rich phase (leucite),
4 not clearly detectable during the SEM and EPMA work, but only in FIB-TEM foils (Figs. 1
5 and 2). Although the areas selected for EPMA looked homogeneous and were larger than the
6 beam spot (1 μm), small leucite solid inclusions undetected during standard SEM imaging
7 probably caused high K concentrations in the Cpx compositional data (Table 1). The leucite
8 inclusions may have been invisible in SEM images due to their small grain size or due to
9 their position immediately below the sample surface. In agreement with recently reviewed
10 data on K-bearing clinopyroxene [18], it is improbable that K can enter the Cpx structure at
11 ambient pressures. Our results have significant implications, especially for the determination
12 of chemical compositions of metal- and metalloid-bearing phases in hazardous waste
13 materials. Standard SEM and EPMA have been routinely used in solid waste characterization
14 over the past two decades. The recent literature contains a large number of papers showing
15 how metals substitute for other cations in the crystalline phases and glass, which are often the
16 predominant constituents of mineral solid wastes. In particular, numerous studies showed that
17 glasses in smelting slags can contain significant amounts of metals. For example, Ettlér et al.
18 [2] reported up to 3.72 wt% PbO and 9.80 wt% ZnO in a matrix glass from Pb slags from
19 Příbram, Czech Republic. Similarly, Piatak et al. [5] showed that interstitial glass in base-
20 metal slags from smelting sites in the U.S.A. can contain up to 5.85 wt% PbO and 4.16 wt%
21 ZnO. However, it is not clear whether these analyses correspond to the actual glass
22 compositions or whether the samples were contaminated by admixtures of metal-rich
23 nanophases. This aspect is very frequent in glasses due to the immiscibility between silicate
24 and sulfide liquids, leading to late solidification of the metal-rich fraction within the residual

1 glass. Another example of Pb smelting slag from Příbram (Czech Republic) is given to
2 illustrate the difficulties associated with the EPMA reliability in waste characterization (Fig.
3 3a and b). The SEM microphotograph in backscattered electrons (BSE) shows metallic
4 inclusions, significantly smaller than 1 μm , dispersed in glass (Fig. 3a and b). These can
5 affect the chemical composition of the glass when analyzed by EPMA. Similarly, Seignez et
6 al. [6] reported the presence of nanometer-scale phases (<60 nm) in glass from the Pb slag,
7 probably corresponding to Fe oxides (wüstite, FeO), and also stressed that SEM/EDS and
8 EPMA results must be interpreted with care. Consequently, these authors proposed the use of
9 methods with higher resolution (TEM) in order to understand the effects of these nanophases
10 on the leaching of contaminants related to the glass dissolution and other weathering
11 processes [6,8]. The same feature is sometimes observed for crystalline phases. Indeed,
12 submicron metal- and metalloid-bearing inclusions were also observed by numerous
13 researchers within the early-crystallizing silicate and oxide phases [2,9,12] (see also Fig. 3a).
14 Although it is known that some substituting elements can enter the structure of crystalline
15 phases (e.g. Zn, Cr, Cu in spinels [2,12,13,21], Zn and Ni in olivines [2,3,9,10] and Zn in
16 melilite [2,9,21]), it is not clear, however, to what extent the EPMA results can be flawed by
17 the presence of nanophases. Melilite is known to contain high concentrations of Zn,
18 corresponding to the hardystonite end-member, $\text{Ca}_2\text{ZnSi}_2\text{O}_7$ [21,22]. For example, in Zn-
19 rich smelting slags from Poland, up to 23 wt% ZnO was reported in melilites [7].
20 Nevertheless, Bindi et al. [22] used TEM for the high-resolution investigation of natural Zn-
21 rich melilite and found that the chemical composition in the sample can be slightly
22 inhomogeneous on a nanoscale, showing the presence of a modulated structure inducing
23 changes in diffraction patterns. Although small amounts of Pb are known to enter the melilite
24 structure [22], it is nevertheless difficult to ascertain whether the reported high Pb

1 concentrations in melilites from slags (up to 52.2 wt% PbO [7]) correspond to substitution in
2 the crystal structure, and this is probably an artifact related to the presence of Pb-rich
3 nanophases. Investigation of secondary alteration products is even more complicated due to
4 the complexity of weathering processes occurring at the waste-water interface. For example,
5 Piantone et al. [15] reported that secondary calcite (CaCO₃) from weathered MSWI bottom
6 ash can contain 0.82 ± 0.43 wt% PbO and up to 0.16 ± 0.19 wt% ZnO. Using EPMA, it is
7 impossible to state whether these metals are incorporated into the calcite structure, adsorbed
8 on the calcite surface, or simply form nano-sized impurities rich in cerussite (PbCO₃) or
9 smithsonite (ZnCO₃) domains. Similarly, Bril et al. [23] studied the secondary alteration
10 products on the surface of Zn slags from Poland and reported EPMA with high
11 concentrations of Zn in anglesite (PbSO₄), barite (BaSO₄) and jarosite (KFe₃(OH)₆(SO₄)₂),
12 which could correspond either to solid-solutions in some cases or to physical impurities.

13

14 **4. Discussion and implications**

15 For mineralogical studies of solid waste materials, it is thus recommended that high-
16 resolution SEM imaging be performed using modes that visualize compositional
17 heterogeneities and to use a SEM instrument with high resolution capability, such as a field
18 emission gun (FEG)-SEM. If a standard SEM instrument is used, particular care with
19 different contrast setting is recommended. Despite their size (<1 μm) approaching the
20 resolution limit of a standard SEM, it is relatively easy to visualize chemically contrasting
21 entities trapped within the material with strikingly different mass (see e.g. metal-bearing
22 droplets in silicate glass in Fig. 3a and b). In contrast, Fig. 3c and d shows more complicated
23 situations with dense metal-rich glass having similar brightness to other associated heavy
24 phases (spinel in Fig. 3c and minute sulfide/metallic droplets in Fig. 3d). In these cases,

1 different contrast settings have to be consecutively employed to visualize all the phases
2 present. As shown in this study, for polyphase materials with grain sizes on a scale of a few
3 micrometers or less, the additional application of TEM, partly coupled to FIB sample
4 preparation, is required in order to obtain reliable compositional information. It is
5 nevertheless important to stress that artifacts of EPMA due to the limited spatial resolution
6 caused by an interaction volume of several μm^3 in size can have a significant impact on
7 modelling of the overall hazardous properties of the particular waste material (e.g., long-term
8 leaching/release of contaminants) and, in justified cases, the solid speciation of contaminants
9 should be verified by other methods with higher resolution (e.g. FIB-TEM).

10

11 **Acknowledgements**

12 This study was supported by the Czech Science Foundation (GA \check{C} CR 210/12/1413), the
13 Ministry of Education, Youth and Sports of the Czech Republic (MSM 0021620855), the
14 Academy of Sciences of the Czech Republic (AV0Z30130516), the Austrian Science Fund
15 (FWF, project I471-N19) and Charles University Student Project (SVV 263203). A number
16 of colleagues helped with the microprobe techniques: Dr. Radek Procházka and Dr. Martin
17 Racek (SEM/EDS), ing. Anna Langrová (EPMA). Dr. Madeleine Štulíková is thanked for
18 correction of the English in the manuscript. The reviews of three anonymous reviewers
19 helped significantly to improve the original version of the manuscript.

20

21

1 **References**

- 2 [1] P. Piantone, Mineralogy and pollutant-trapping mechanisms, *C. R. Geosci.* 336 (2004)
3 1415–1416.
- 4 [2] V. Ettlér, O. Legendre, F. Bodéan, J.C. Touray, Primary phases and natural weathering
5 of old lead-zinc pyrometallurgical slag from Příbram, Czech Republic, *Can. Mineral.*
6 39 (2001) 873–888.
- 7 [3] A. Manasse, M. Mellini, C. Viti, The copper slags of the Capattoli Valley, Campiglia
8 Marittima, Italy. *Eur. J. Mineral.* 13 (2001) 949–960.
- 9 [4] V. Ettlér, Z. Johan, Mineralogy of metallic phases in sulphide matte from primary lead
10 smelting, *C. R. Geosci.* 335 (2003) 1005–1012.
- 11 [5] N.M. Piatak, R.R. Seal II, J.M. Hammarstrom, Mineralogical and geochemical controls
12 on the release of trace elements from slag produced by base- and precious-metal
13 smelting at abandoned mine sites, *Appl. Geochem.* 19 (2004) 1039–1064.
- 14 [6] N. Seignez, A. Gauthier, D. Bulteel, M. Buatier, P. Recourt, D. Damidot, J.L. Potdevin
15 Effect of Pb-rich and Fe-rich entities during alteration of a partially vitrified
16 metallurgical waste, *J. Hazard. Mater.* 149 (2007) 418–431.
- 17 [7] J. Puziewicz, K. Zainoun, H. Bril, Primary phases in pyrometallurgical slags from a zinc-
18 smelting waste dump, Świętochłowice, Upper Silesia, Poland, *Can. Mineral.* 45
19 (2007) 1189–1200.
- 20 [8] N. Seignez, A. Gauthier, D. Bulteel, D. Damidot, J.L. Potdevin, Leaching of lead
21 metallurgical slags and pollutant mobility far from equilibrium conditions, *Appl.*
22 *Geochem.* 23 (2008) 3699–3711.

- 1 [9] J. Kierczak, C. Néel, J. Puziewicz, H. Bril, The mineralogy and weathering of slag
2 produced by the smelting of lateritic Ni ores, Szklary, southwestern Poland, *Can.*
3 *Mineral.* 47 (2009) 557–572.
- 4 [10] V. Ettler, Z. Johan, B. Kříbek, O. Šebek, M. Mihaljevič, Mineralogy and environmental
5 stability of slags from the Tsumeb smelter, Namibia, *Appl. Geochem.* 24 (2009) 1–15.
- 6 [11] V. Ettler, R. Červinka, Z. Johan, Mineralogy of medieval slags from lead and silver
7 smelting (Bohutín, Příbram district, Czech Republic): Towards estimation of
8 historical smelting conditions, *Archaeometry* 51 (2009) 987–1007.
- 9 [12] M. Vítková, V. Ettler, Z. Johan, B. Kříbek, O. Šebek, M. Mihaljevič, Primary and
10 secondary phases in copper-cobalt smelting slags from the Copperbelt Province,
11 Zambia, *Mineral. Mag.* 74 (2010) 581–600.
- 12 [13] N.M. Piatak, R.R. Seal II, Mineralogy and the release of trace elements from slag from
13 the Hegeler Zinc smelter, Illinois (USA). *Appl. Geochem.* 25 (2010) 302–320.
- 14 [14] P. Piantone, F. Bodéan, R. Derie, G. Depelsenaire, Monitoring the stabilization of
15 municipal solid waste incineration fly ash by phosphation: mineralogical and balance
16 approach, *Waste Manage.* 23 (2003) 225–243.
- 17 [15] P. Piantone, F. Bodéan, L. Chatelet-Snidaro, Mineralogical study of secondary mineral
18 phases from weathered MSWI bottom ash: implications for the modelling and trapping
19 of heavy metals, *Appl. Geochem.* 19 (2004) 1891–1904.
- 20 [16] A.B. Hernandez, J.H. Ferrasse, P. Chaurand, H. Saveyn, D. Borschneck, N. Roche,
21 Mineralogy and leachability of gasified sewage sludge solid residues, *J. Hazard.*
22 *Mater.* 191 (2011) 219–227.
- 23 [17] P.J. Potts, J.F.W. Bowles, S.J.B. Reed, M.R. Cave, *Microprobe Techniques in the Earth*
24 *Sciences*, The Mineralogical Society series 6, Chapman & Hall, London, 1995.

- 1 [18] O.G. Safonov, L. Bindi, V.L. Vinograd, Potassium-bearing clinopyroxene: a review of
2 experimental, crystal chemical and thermodynamic data with petrological
3 applications, *Mineral. Mag.* 75 (2011) 2467–2484.
- 4 [19] R.D. Shannon, Revised effective ionic radii and systematic studies of interatomic
5 distances in halides and chalcogenides, *Acta Cryst.* A32 (1976) 453–443.
- 6 [20] J.L. Lábár, Consistent indexing of a (set of) SAED pattern(s) with the Process
7 Diffraction program, *Ultramicroscopy* 103 (2005) 237–249.
- 8 [21] A. Trujillo-Vazquez, H. Metiver-Pignon, L. Tiruta-Barna, P. Piantone, Characterization
9 of a mineral waste resulting from the melting treatment of air pollution control
10 residues, *Waste Manage.* 29 (2009) 530–538.
- 11 [22] L. Bindi, M. Czank, F. Röthlisberger, P. Bonazzi, Hardystonite from Franklin Furnace: a
12 natural modulated melilite, *Am. Mineral.* 86 (2001) 747–751.
- 13 [23] H. Bril, K. Zainoun, J. Puziewicz, A. Courtin-Nomade, M. Vanaecker, J.C. Bollinger,
14 Secondary phases from the alteration of a pile of zinc-smelting slags as indicators of
15 environmental conditions. An example from Świętochłowice, Upper Silesia, Poland,
16 *Can. Mineral.* 46 (2008) 1235–1248.

Table 1. Representative electron microprobe analyses of plume-like clinopyroxenes (in wt% of oxides) and empirical formulae calculated to 4 cations and 6 oxygens per formula unit.

wt%	spot 2	spot 23	Range ($n = 11$)
SiO ₂	43.73	44.54	43.15-44.54
TiO ₂	0.59	0.61	0.54-0.7
Al ₂ O ₃	7.63	7.84	6.42-7.84
Cr ₂ O ₃	< DL	< DL	< DL-0.18
FeO	19.35	18.87	18.54-21.94
MgO	3.81	4.32	3.81-4.79
CoO	1.30	1.29	1.16-1.56
CaO	18.80	19.23	18.8-21.34
Na ₂ O	0.27	0.15	< DL-0.27
K ₂ O	2.88	1.98	0.62-2.88
Total	98.36	98.83	98.36-100.9
<i>T site</i>			
Si	1.742	1.765	1.705-1.765
^[4] Al	0.258	0.235	0.235-0.295
^[4] Fe ³⁺	n.d.	n.d.	n.d.
<i>M1 site</i>			
^[6] Al	0.100	0.132	0.014-0.132
^[6] Fe ³⁺	0.290	0.178	0.177-0.328
Ti	0.018	0.018	0.016-0.021
Cr	n.d.	n.d.	n.d.-0.006
Co	0.042	0.041	0.037-0.050
Mg	0.226	0.255	0.226-0.283
Fe ²⁺	0.325	0.376	0.323-0.400
<i>M2 site</i>			
Fe ²⁺	0.030	0.072	0.030-0.078
Ca	0.802	0.817	0.802-0.908
Na	0.021	0.012	n.d.-0.021
K	0.146	0.100	0.031-0.146

< DL – below detection limit;
n.d. – not determined

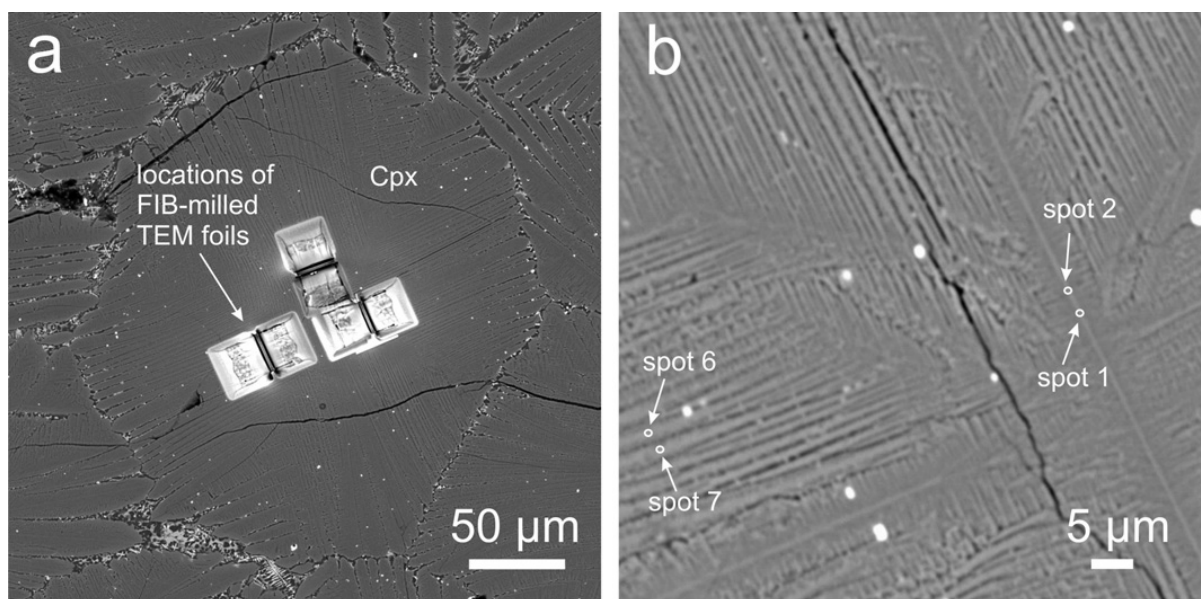


Figure 1. SEM-BSE (back scattered electron) images (a) of clinopyroxene (Cpx) plumes and (b) zoom on individual Cpx lamellae from the Cu smelting slag with location of several EPMA spots.

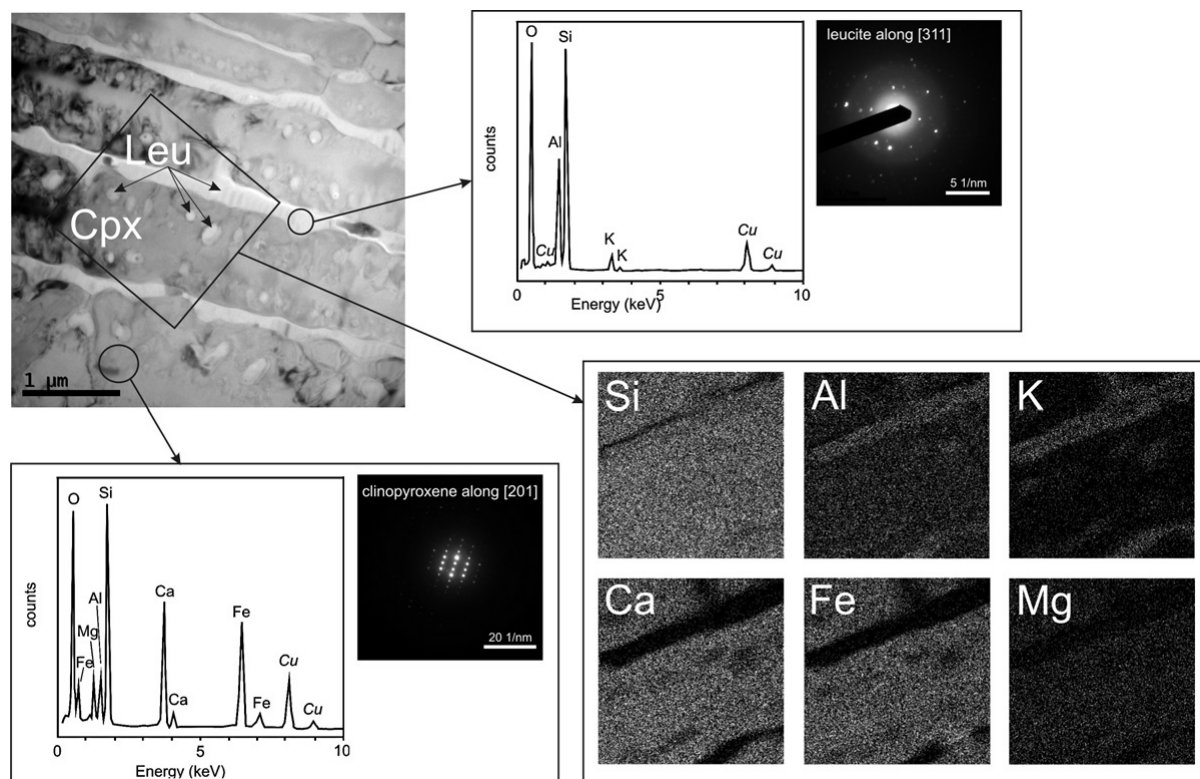


Figure 2. TEM image of the FIB-prepared foil oriented perpendicular to the Cpx lamellae. The presence of leucite (Leu) trapped within the Cpx can be discerned. The individual phases were identified by SAED and EDS (Cu given in italics, being present in the TEM grid); the X-ray elemental maps show the spatial distribution of the major elements within a given zone.

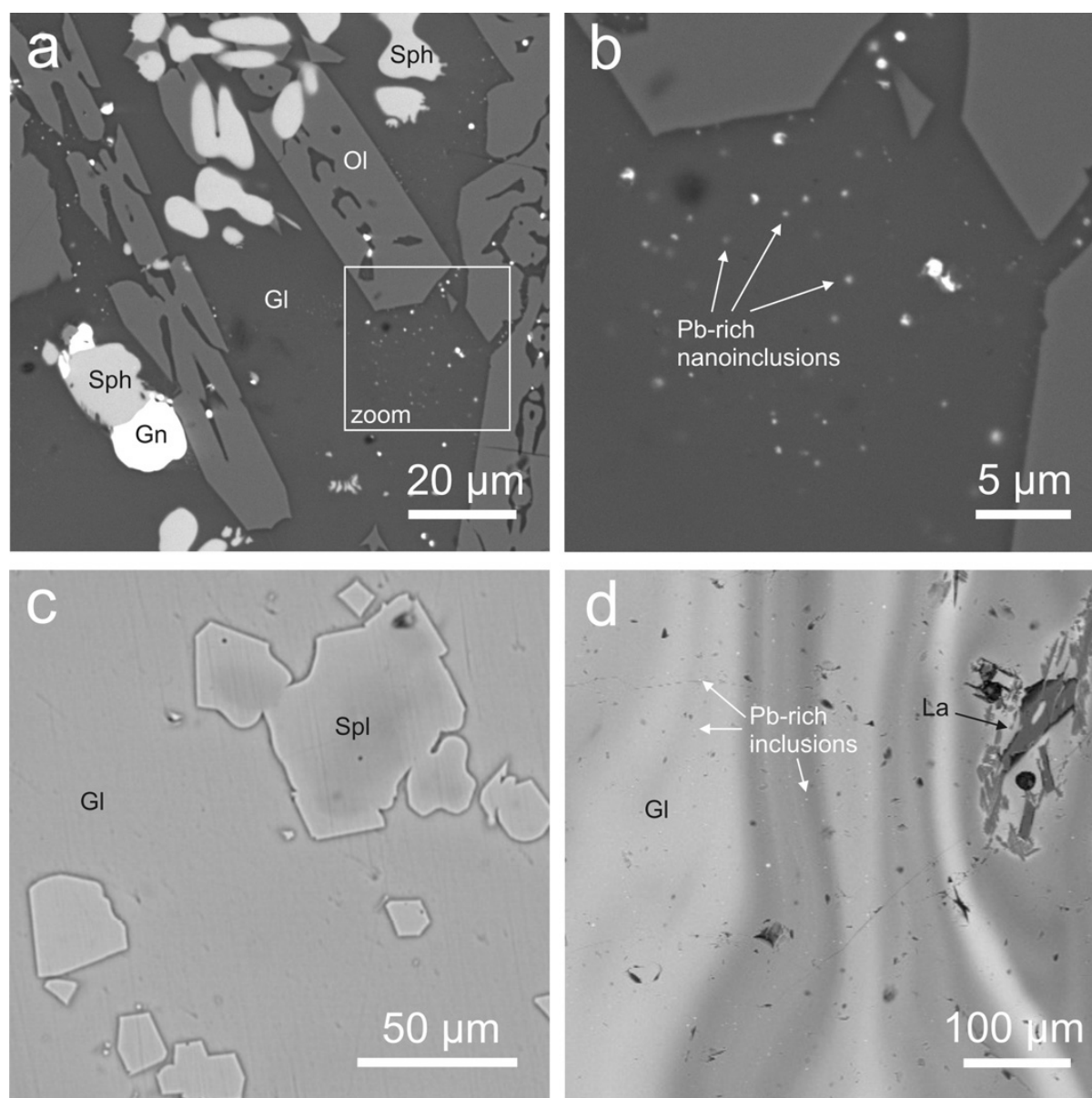


Figure 3. SEM-BSE images of the base-metal smelting slags. (a) Typical assemblage of Pb slag composed of olivine (Ol), glass (Gl), sphalerite (Sph) and galena (Gn) (slag from P^řibram, Czech Republic); (b) zoom on a glassy zone with nano-sized Pb-rich inclusions, which can affect the reliability of EPMA analyses of the glass; (c) metal-rich glass (7.85 wt% PbO, 9.12 wt% ZnO, 1.78 wt% CuO) with similar contrast as spinels (Spl) (slag from Tsumeb, Namibia, adapted from [10]); (d) difficult setting of contrast in an SEM image of Pb-rich glass (up to 33 wt% PbO) embedding small sulfide/metallic inclusions and associated to larnite, Ca₂SiO₄ (La) (medieval slag from an archaeological site in Prague, Czech Republic).